

# Universal Adversarial Perturbations for CNN Classifiers in EEG-Based BCIs

Zihan Liu, Xiao Zhang and Dongrui Wu

**Abstract**—Multiple convolutional neural network (CNN) classifiers have been proposed for electroencephalogram (EEG) based brain-computer interfaces (BCIs). However, CNN models have been found vulnerable to universal adversarial perturbations (UAPs), which are small and example-independent, yet powerful enough to degrade the performance of a CNN model, when added to a benign example. This paper proposes a novel total loss minimization (TLM) approach to generate UAPs for EEG-based BCIs. Experimental results demonstrate the effectiveness of TLM on three popular CNN classifiers for both target and non-target attacks. We also verify the transferability of UAPs in EEG-based BCI systems. To our knowledge, this is the first study on UAPs of CNN classifiers in EEG-based BCIs, and also the first study on UAPs for target attacks. UAPs are easy to construct, and can attack BCIs in real-time, exposing a critical security concern of BCIs.

**Index Terms**—Brain-computer interface, convolutional neural network, electroencephalogram, universal adversarial perturbation

## I. INTRODUCTION

A brain-computer interface (BCI) enables people to interact directly with a computer using brain signals. Due to its low-cost and convenience, electroencephalogram (EEG), which records the brain’s electrical activities from the scalp, has become the most widely used input signal in BCIs. There are several popular paradigms in EEG-based BCIs, e.g., P300 evoked potentials [1]–[4], motor imagery (MI) [5], steady-state visual evoked potentials [6], etc.

Deep learning, which eliminates manual feature engineering, has become increasingly popular in decoding EEG signals in BCIs. Multiple convolutional neural network (CNN) classifiers have been proposed for EEG-based BCIs. Lawhern *et al.* [7] proposed EEGNet, a compact CNN model demonstrating promising performance in several EEG-based BCI tasks. Schirrmester *et al.* [8] proposed a deep CNN model (DeepCNN) and a shallow CNN model (ShallowCNN) for EEG classification. There were also studies that converted EEG signals to spectrograms or topoplots and then fed them into deep learning classifiers [9]–[11]. This paper focuses on CNN classifiers which take raw EEG signals as the input, but our approach should also be extendable to other forms of inputs.

Z. Liu, X. Zhang and D. Wu are with the Key Laboratory of the Ministry of Education for Image Processing and Intelligent Control, School of Artificial Intelligence and Automation, Huazhong University of Science and Technology, Wuhan 430074, China. Email: zhliu95@hust.edu.cn, xiao\_zhang@hust.edu.cn, drwu@hust.edu.cn.

The first two authors contributed equally to this work.  
D. Wu is the corresponding author.

Albeit their promising performance, it was found that deep learning models are vulnerable to adversarial attacks [12], [13], in which deliberately designed tiny perturbations can significantly degrade the model performance. Many successful adversarial attacks have been reported in image classification [14]–[17], speech recognition [18], malware detection [19], etc.

In many practical BCI systems, EEG signals are sent from the EEG headset through wires or wirelessly to a computer, a smart phone, or the cloud, for analysis. Thus, an attacker can tamper with the EEG signals before or during their transmission, e.g., attaching a jamming module to the EEG headset signal transmitter, as shown in Fig. 1.

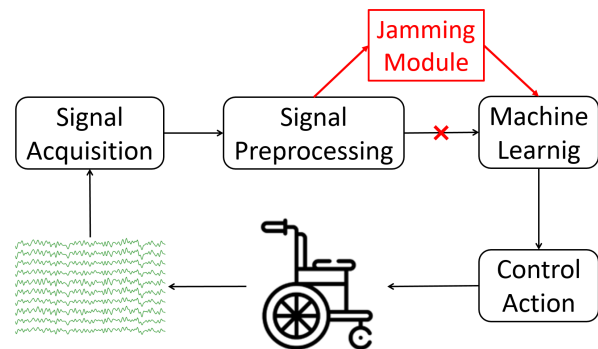


Fig. 1. Attacking an EEG-based BCI system.

Zhang and Wu [20] were the first to discover that adversarial examples also exist in EEG-based BCI systems. They successfully attacked three CNN classifiers (EEGNet, DeepCNN, and ShallowCNN) in three different scenarios (white-box, gray-box, and black-box). These results exposed a critical security problem in EEG-based BCIs, which had not been investigated before. As pointed out in [20], “*EEG-based BCIs could be used to control wheelchairs or exoskeleton for the disabled [21], where adversarial attacks could make the wheelchair or exoskeleton malfunction. The consequence could range from merely user confusion and frustration, to significantly reducing the user’s quality of life, and even to hurting the user by driving him/her into danger on purpose. In clinical applications of BCIs in awareness evaluation/detection for disorder of consciousness patients [21], adversarial attacks could lead to misdiagnosis.*”

Albeit their great success, Zhang and Wu’s approaches [20] had the following limitations:

- 1) An adversarial perturbation needs to be computed specifically for each input EEG trial, which is inconvenient.

- 2) To compute the adversarial perturbation, the attacker needs to know the complete EEG trial in advance, and hence it is impossible to perform the attack as soon as the EEG trial starts.

This paper introduces universal adversarial perturbation (UAP), which is a universal perturbation template computed offline and can be added to any EEG trial in real-time. So, it avoids the above two limitations simultaneously.

Studies on UAPs appeared in the literature very recently. Moosavi-Dezfooli *et al.* [22] discovered the existence of UAPs, and verified that they can fool state-of-the-art machine learning models in image classification. Their method for crafting the UAPs, based on DeepFool [23], solves a complex optimization problem. The same idea was later used in attacking speech recognition systems [24]. Behjati *et al.* [25] proposed a gradient projection based approach for generating UAPs in text classification. Mopuri *et al.* [26] proposed a generalizable and data-free approach for crafting UAPs, which is independent of the underlying task.

This paper investigates UAPs in EEG-based BCIs. We make the following three contributions:

- 1) To our knowledge, this is the first study on UAPs for EEG-based BCIs, which make adversarial attacks in BCIs more convenient and more practical.
- 2) We propose a novel total loss minimization (TLM) approach for generating a UAP for EEG trials, which can achieve better attack performance with a smaller perturbation, compared with the traditional DeepFool based approach.
- 3) Our proposed TLM can perform both non-target attacks and target attacks. To our knowledge, no one has studied UAPs for target attacks before.

The remainder of this paper is organized as follows: Section II introduces two approaches to generate UAPs for EEG trials. Section III describes our experimental setting. Sections IV and V present the experimental results on non-target attacks and target attacks, respectively. Finally, Section VI draws conclusions and points out several future research directions.

## II. UNIVERSAL ADVERSARIAL PERTURBATIONS (UAPs)

This section first introduces an iterative algorithm for crafting a UAP for EEG trials, then presents the details of our proposed TLM approach. All source code can be downloaded at [https://github.com/ZihanLiu95/UAP\\_EEG](https://github.com/ZihanLiu95/UAP_EEG).

We distinguish between two types of attacks:

- *Target attacks*, in which the attacker wants all adversarial examples to be classified into a *specific* class. For example, for 3-class MI (left-hand, right-hand, and feet), the attacker may want all left-hand and right-hand adversarial trials to be misclassified as feet trials.
- *Non-target attacks*, in which the attacker wants the adversarial examples to be misclassified, but does not care which class they are classified into. In the above example, a left-hand adversarial trial could be misclassified as a right-hand trial, or a feet trial.

### A. Problem Setup

To attack a BCI system, the adversarial perturbations need to be added to benign EEG signals in real-time.

Let  $X_i \in \mathbb{R}^{C \times T}$  be the  $i$ -th raw EEG trial ( $i = 1, \dots, n$ ), where  $C$  is the number of EEG channels and  $T$  the number of time domain samples. Let  $\mathbf{x} \in \mathbb{R}^{C \cdot T \times 1}$  be the vector form of  $X_i$ , which concatenates all columns of  $X_i$  into a single column. Let  $k(\mathbf{x}_i)$  be the estimated label from the target CNN model,  $\mathbf{v} \in \mathbb{R}^{C \cdot T \times 1}$  the UAP,  $\tilde{\mathbf{x}}_i = \mathbf{x}_i + \mathbf{v}$  the adversarial EEG trial after adding the UAP. Then,  $\mathbf{v}$  needs to satisfy:

$$\left. \begin{aligned} \frac{1}{n} \sum_{i=1}^n I(k(\mathbf{x}_i + \mathbf{v}) \neq k(\mathbf{x}_i)) &\geq \delta \\ \|\mathbf{v}\|_p &\leq \xi \end{aligned} \right\}, \quad (1)$$

where  $\|\cdot\|_p$  is the  $L_p$  norm, and  $I(\cdot)$  is the indicator function which equals 1 if its argument is true, and 0 otherwise. The parameter  $\delta \in (0, 1]$  determines the desired attack success rate (ASR), and  $\xi$  constrains the magnitude of  $\mathbf{v}$ . Briefly speaking, the first constraint requires the UAP to achieve a desired ASR, and the second constraint ensures the UAP is small.

Next, we describe how a UAP can be crafted for EEG data. We first introduce DeepFool [23], a white-box attack (the attacker has access to all information of the victim model, including its architecture and parameters) approach for crafting an adversarial perturbation for a *single* input example, and then extend it to crafting a UAP for *multiple* examples. Finally, we propose a novel TLM approach to craft UAP, which can be applied to both non-target attacks and target attacks.

### B. DeepFool-Based UAP

DeepFool is an approach for crafting an adversarial perturbation for a single input example.

Consider a binary classification problem, where the labels are  $\{-1, 1\}$ . Let  $\mathbf{x}$  be an input example, and  $f$  an affine classification function  $f(\mathbf{x}) = \mathbf{w}^T \mathbf{x} + b$ . Then, the predicted label is  $k(\mathbf{x}) = \text{sign}f(\mathbf{x})$ . The minimal adversarial perturbation  $\mathbf{r}^*$  should move  $\mathbf{x}$  to the decision hyperplane  $\mathcal{F} = \{\mathbf{x}^* : \mathbf{w}^T \mathbf{x}^* + b = 0\}$ , i.e.,

$$\mathbf{r}^* = -\frac{f(\mathbf{x})}{\|\mathbf{w}\|_2} \mathbf{w}. \quad (2)$$

CNN classifiers are nonlinear. So, an iterative procedure [23] is used to identify the adversarial perturbation, by treating  $f$  approximately linear around  $\mathbf{x}_t$  at Iteration  $t$ . Then, the minimal perturbation at Iteration  $t$  is computed as:

$$\min_{\mathbf{r}_t} \|\mathbf{r}_t\|, \quad \text{s.t. } f(\mathbf{x}_t) + \nabla f(\mathbf{x}_t)^T \mathbf{r}_t = 0. \quad (3)$$

The perturbation  $\mathbf{r}_t$  at Iteration  $t$  is computed using the closed-form solution in (2), and then  $\mathbf{x}_{t+1} = \mathbf{x}_t + \mathbf{r}_t$  is used in the next iteration. The iteration stops when  $\mathbf{x}_{t+1}$  starts to change the classification label. The pseudocode is given in Algorithm 1.

Algorithm 1 can be extended to multi-class classification by using the one-versus-all scheme to find the closest hyperplane. Experiments in [23] demonstrated that DeepFool can achieve comparable attack performance as the fast gradient sign method (FGSM) [14], but the magnitude of the perturbation is smaller, which is more desirable.

---

**Algorithm 1:** DeepFool [23] for generating an adversarial perturbation for a *single* input example.

---

**Input:**  $\mathbf{x}$ , an input example;  
 $f$ , the classification function.  
**Output:**  $\mathbf{r}^*$ , the adversarial perturbation.  
 $\mathbf{x}_0 = \mathbf{x}$ ;  
 $t = 0$ ;  
**while**  $\text{sign}f(\mathbf{x}_t) \neq \text{sign}f(\mathbf{x}_0)$  **do**  
     $\mathbf{r}_t = -\frac{f(\mathbf{x}_t)}{\|\nabla f(\mathbf{x}_t)\|_2} \nabla f(\mathbf{x}_t)$ ;  
     $\mathbf{x}_{t+1} = \mathbf{x}_t + \mathbf{r}_t$ ;  
     $t = t + 1$ ;  
**end**  
 $\mathbf{r}^* = \sum_{i=0}^t \mathbf{r}_i$ .

---

UAPs were recently discovered in image classification by Moosavi-Dezfooli *et al.* [22], who showed that a fixed adversarial perturbation can fool multiple state-of-the-art CNN classifiers on multiple images. They developed a DeepFool-based iterative algorithm to craft the UAP, which satisfies (1). A UAP is designed by proceeding iteratively over all examples in the dataset  $\mathbf{X} = \{\mathbf{x}_i\}_{i=1}^n$ . In each iteration, DeepFool is used to compute a minimum perturbation  $\Delta \mathbf{v}_i$  for the current perturbed point  $\mathbf{x}_i + \mathbf{v}$ , and then  $\Delta \mathbf{v}_i$  is aggregated into  $\mathbf{v}$ .

More specifically, if the current universal perturbation  $\mathbf{v}$  cannot fool the classifier on  $\mathbf{x}_i$ , then a minimum extra perturbation  $\Delta \mathbf{v}_i$  that can fool  $\mathbf{x}_i$  is computed by solving the following optimization problem:

$$\min_{\Delta \mathbf{v}_i} \|\Delta \mathbf{v}_i\|_2, \quad \text{s.t. } k(\mathbf{x}_i + \mathbf{v} + \Delta \mathbf{v}_i) \neq k(\mathbf{x}_i). \quad (4)$$

To ensure the constraint  $\|\mathbf{v}\|_p \leq \xi$  is satisfied, the updated universal perturbation  $\mathbf{v}$  is further projected onto the  $\ell_p$  ball of radius  $\xi$  centered at 0. The projection operator  $\mathcal{P}_{p,\xi}$  is defined as:

$$\mathcal{P}_{p,\xi}(\mathbf{v}) = \arg \min_{\|\mathbf{v}'\|_p \leq \xi} \|\mathbf{v} - \mathbf{v}'\|_2. \quad (5)$$

Then, the UAP can be updated by  $\mathbf{v} = \mathcal{P}_{p,\xi}(\mathbf{v} + \Delta \mathbf{v}_i)$  in each iteration. This process is repeated on the entire dataset until the maximum number of iterations is reached, or the ASR on the perturbed dataset  $\mathbf{X}_v = \{\mathbf{x}_i + \mathbf{v}\}_{i=1}^n$  exceeds the target ASR threshold  $\delta \in (0, 1]$ , i.e.,

$$\text{ASR}(\mathbf{X}_v, \mathbf{X}) = \frac{1}{n} \sum_{i=1}^n I(k(\mathbf{x}_i + \mathbf{v}) \neq k(\mathbf{x}_i)) \geq \delta. \quad (6)$$

The pseudo-code of the DeepFool-based algorithm is given in Algorithm 2.

### C. TLM-Based UAP

Different from the DeepFool-based algorithm, TLM directly optimizes an objective function w.r.t. the UAP by batch gradient descent. In white-box attacks, the parameters of the victim model are known and fixed, and hence we can view the UAP as a variable to minimize an objective function on the entire training set.

---

**Algorithm 2:** DeepFool-based algorithm for generating a UAP [22].

---

**Input:**  $\mathbf{X} = \{\mathbf{x}_i\}_{i=1}^n$ ,  $n$  input examples;  
 $k$ , the classifier;  
 $\xi$ , the maximum  $\ell_p$  norm of the UAP;  
 $\delta$ , the desired ASR;  
 $M$ , the maximum number of iterations.  
**Output:**  $\mathbf{v}$ , a UAP.  
 $\mathbf{v} = \mathbf{0}$ ;  
 $\mathbf{X}_v = \mathbf{X}$ ;  
**for**  $m = 1, \dots, M$  **do**  
    **if**  $\text{ASR}(\mathbf{X}_v, \mathbf{X}) < \delta$  **then**  
        **for** *Each*  $\mathbf{x}_i \in \mathbf{X}$  **do**  
            **if**  $k(\mathbf{x}_i + \mathbf{v}) == k(\mathbf{x}_i)$  **then**  
                Use DeepFool to compute the minimal perturbation  $\Delta \mathbf{v}_i$  in (4);  
                Update the perturbation by (5):  
                 $\mathbf{v} \leftarrow \mathcal{P}_{p,\xi}(\mathbf{v} + \Delta \mathbf{v}_i)$ ;  
            **end**  
        **end**  
         $\mathbf{X}_v = \{\mathbf{x}_i + \mathbf{v}\}_{i=1}^n$ ;  
    **else**  
        Break;  
    **end**  
**end**  
**Return**  $\mathbf{v}$ .

---

Specifically, we solve the following optimization problem:

$$\min_{\mathbf{v}} E_{\mathbf{x} \sim \mathcal{D}} l(\mathbf{x} + \mathbf{v}, y) + \alpha \cdot C(\mathbf{x}, \mathbf{v}), \quad \text{s.t. } \|\mathbf{v}\|_p \leq \xi, \quad (7)$$

where  $l(\mathbf{x} + \mathbf{v}, y)$  is a loss function, in which  $y$  is the (true or predicted) label of example  $\mathbf{x}$ ,  $C(\mathbf{x}, \mathbf{v})$  the constraint on the perturbation  $\mathbf{v}$ , and  $\alpha$  the regularization coefficient. Our proposed approach is highly flexible, as the attacker can choose different optimizers, loss functions, or constraints, according to the specific task.

Our approach can be applied to both target and non-target attacks by simply updating the loss function  $l$ .

For non-target attacks, the loss function  $l$  can be defined as:

$$l(\mathbf{x}, y) = \log(p_y(\mathbf{x})), \quad (8)$$

where  $p_y(\mathbf{x})$  is the predicted probability corresponding to the true label  $y$ . We could also use  $\arg \max_j p_j(\mathbf{x})$ , i.e., the predicted label, to replace  $y$  if the true label is not available.

For target attacks, we force the model to classify an adversarial example into a specific class, and hence  $l$  can be defined as:

$$l(\mathbf{x}, y) = -\log(p_y(\mathbf{x})), \quad (9)$$

where  $y$  is the target label (which is usually different from the true label) the attacker wants.

Note that the only difference between (8) and (9) is that there is a minus sign in (9), because in non-target attacks we want to *minimize* the predicted probability for the *true* class, whereas in target attacks we want to *maximize* the predicted probability for the *target* class.

There are also various options for the constraint function  $C(\mathbf{x}, \mathbf{v})$ . In most cases, we can simply set  $C(\mathbf{x}, \mathbf{v})$  as L1 or L2 regularization on the UAP  $\mathbf{v}$ ; however, it can also be a more sophisticated function, e.g., a metric function to detect whether the input is an adversarial example or not. When a new metric function for detecting adversarial examples is proposed, our approach can also be utilized to test its reliability: we set  $C$  as the metric function to check whether we can still find an adversarial example. Given the diversity of metric functions, we only consider L1 or L2 regularization in this paper. Other metric functions and defense strategies for TLM-UAP will be considered in our future research.

The pseudo-code of our proposed TLM approach is given in Algorithm 3.

---

**Algorithm 3:** The proposed TLM approach for generating a UAP.

---

**Input:**  $\mathbf{X}_{train} = \{\mathbf{x}_{train,i}\}_{i=1}^n$ ,  $n$  training examples;  
 $\mathbf{X}_{val} = \{\mathbf{x}_{val,i}\}_{i=1}^m$ ,  $m$  validation examples;  
 $k$ , the classifier;  
 $\xi$ , the maximum  $\ell_p$  norm of the UAP;  
 $\alpha$ , the regularization coefficient;  
 $\delta$ , the desired ASR;  
 $M$ , the maximum number of epoches;

**Output:**  $\mathbf{v}_{best}$ , a UAP.

$\mathbf{v} = \mathbf{0}$ ;

$r = 0$ ;

**for**  $m = 1, \dots, M$  **do**

**for** Each mini-batch  $\mathbf{D} \in \mathbf{X}_{train}$  **do**

        Update  $\mathbf{v}$  in (7) for  $\mathbf{D}$  with an optimizer;

        Constrain  $\mathbf{v}$  by (5):  $\mathbf{v} \leftarrow \mathcal{P}_{p,\xi}(\mathbf{v})$ ;

**end**

$\mathbf{X}_{val,\mathbf{v}} = \{\mathbf{x}_{val,i} + \mathbf{v}\}_{i=1}^m$ ;

**if**  $ASR(\mathbf{X}_{val,\mathbf{v}}, \mathbf{X}_{val}) > r$  **then**

$r = ASR(\mathbf{X}_{val,\mathbf{v}}, \mathbf{X}_{val})$ ;

$\mathbf{v}_{best} = \mathbf{v}$ ;

**end**

**if**  $R > \delta$  **then**

        Break;

**end**

**end**

**Return**  $\mathbf{v}_{best}$ .

---

### III. EXPERIMENTAL SETTINGS

This section introduces the experimental settings for validating the performance of our proposed TLM approach.

#### A. The Three BCI Datasets

The following three BCI datasets were used in our experiments, as in [20], [27]:

**P300 evoked potentials (P300):** The P300 dataset, first introduced in [28], contained eight subjects. In the experiment, each subject faced a laptop on which six images were flashed randomly to elicit P300 responses. The goal was to classify whether the image was a target or non-target. The 32-channel EEG data was downsampled to 256Hz, bandpass filtered to

[1, 40] Hz, and epoched to [0, 1]s after each image onset. Then, we normalized the data using  $\frac{x - \text{mean}(x)}{10}$ , and clipped the resulting values to [-5, 5]. Each subject had about 3,300 trials.

**Feedback error-related negativity (ERN):** The ERN dataset [29] was used in a Kaggle challenge<sup>1</sup>. The EEG signals were collected from 26 subjects and consisted of two classes (bad-feedback and good-feedback). The entire dataset was partitioned into a training set (16 subjects) and a test set (10 subjects). We only used the 16 subjects in the training set as we had no access to the test set. The 56-channel EEG signals were downsampled to 200Hz, bandpass filtered to [1, 40]Hz, epoched to [0, 1.3]s after each stimulus, and  $z$ -normalized. Each subject had 340 trials.

**Motor imagery (MI):** The MI dataset was Dataset 2A<sup>2</sup> in BCI Competition IV [30]. The EEG signals were collected from nine subjects and consisted of four classes: the imagined movements of the left hand, right hand, both feet, and tongue. The 22-channel EEG signals were downsampled to 128Hz, bandpass filtered to [4, 40]Hz, epoched to [0, 2]s after each imagination prompt, and standardized using an exponential moving average window with a decay factor of 0.999, as in [7]. Each subject had 576 trials, with 144 in each class.

#### B. The Three CNN Models

The following three CNN models were used in our experiments, as in [20], [27]:

**EEGNet:** EEGNet [7] is a compact CNN architecture for EEG-based BCIs. It consists of two convolutional blocks and a classification block. To reduce the number of model parameters, EEGNet uses depthwise and separable convolutions [31] instead of traditional convolutions.

**DeepCNN:** DeepCNN [8] consists of four convolutional blocks and a softmax layer for classification, which is deeper than EEGNet. Its first convolutional block is specially designed to handle EEG inputs, and the other three are standard convolutional blocks.

**ShallowCNN:** Inspired by filter bank common spatial patterns [32], ShallowCNN [8] is specifically tailored to decode band power features. Compared with DeepCNN, ShallowCNN uses a larger kernel in temporal convolution, and then a spatial filter, squaring nonlinearity, a mean pooling layer and logarithmic activation function.

#### C. The Two Experimental Settings

We considered two experimental settings:

**Within-subject experiments:** For each individual subject, EEG trials were shuffled and divided into 80% training and 20% test. We further randomly sampled 25% trials from the training set as the validation set in early stopping.

**Cross-subject experiments:** For each dataset, leave-one-subject-out cross-validation was performed. Assume a dataset had  $N$  subjects, and the  $N$ -th subject was selected as the test subject. In training, trials from the first  $N - 1$  subjects were

<sup>1</sup><https://www.kaggle.com/c/inria-bci-challenge>

<sup>2</sup><http://www.bci.de/competition/iv/>

mixed, shuffled, and divided into 75% for training and 25% for validation in early stopping.

When training the victim models on the first two datasets, we applied weights to different classes to accommodate the class imbalance, according to the inverse of its proportion in the training set. We used the cross entropy loss function and Adam optimizer [33]. Early stopping was used to reduce overfitting.

The parameters for generating DF-UAP and TLM-UAP are shown in Table I. It should be noted that TLM-UAP was trained with an L2 constraint, and hence there is no need to worry about the magnitude of the perturbation increasing with the training iteration. Therefore, we set  $\delta$  to 1.0 and used early stopping (patience=10) to decide whether to stop the iteration or not. We also replaced the true labels with the predicted ones, as in real-world applications we do not have the true labels.

TABLE I  
PARAMETERS FOR GENERATING DF-UAP AND TLM-UAP.  $\|v\|_\infty$  WAS USED IN COMPUTING THE NORM OF THE UAPS.

|         | $\xi$ | $\delta$ | $M$ | $\alpha$ | Constraint |
|---------|-------|----------|-----|----------|------------|
| DF-UAP  | 0.2   | 0.8      | 10  | -        | -          |
| TLM-UAP | 0.2   | 1.0      | 500 | 100      | L2         |

#### D. The Two Performance Measures

Both raw classification accuracy (RCA) and balanced classification accuracy (BCA) [3] were used as the performance measures. The RCA is the ratio of the number of correctly classified samples to the number of total samples, and the BCA is the average of the individual RCAs of different classes.

The BCA is necessary, because some BCI paradigms (e.g., P300) have intrinsic significant class imbalance, and hence using RCA alone may be misleading sometimes.

### IV. NON-TARGET ATTACK RESULTS

This section presents the experimental results in non-target attacks on the three BCI datasets. Recall that a non-target attack forces a model to misclassify an adversarial example to any class, instead of a specific class.

For notation convenience, we denote the UAP generated by the DeepFool-based algorithm (Algorithm 2) as *DF-UAP*, and the UAP generated by the proposed TLM (Algorithm 3) as *TLM-UAP*.

#### A. Baseline Performances

We compared the UAP attack performance with two baselines:

1) *Clean Baseline*: We evaluated the baseline performances of the three CNN models on the clean (unperturbed) EEG data, as shown in the first part of Table II. For all three datasets and all three classifiers, generally RCAs and BCAs of the within-subject experiments were higher than their counterparts in the cross-subject experiments, which is reasonable, since individual differences cause inconsistency among EEG trials from different subjects.

2) *Noisy Baseline*: We added uniform random noise  $0.2 \cdot U(-1, 1)$  to the original EEG data. If the random noise under the same magnitude constraint can significantly degrade the classification performance, then there is no need to compute a UAP. The results are shown in Table II. Random noise did not degrade the classification performance in most cases, except sometimes on the MI dataset. This suggests that the three CNN classifiers are generally robust to random noise, therefore we should deliberately design the adversarial perturbations.

#### B. White-Box Non-target Attack Performances

First consider white-box attacks, where we have access to all information of the victim model, including its architecture and parameters. The performances of DF-UAP and TLM-UAP in white-box non-target attacks are shown in the second part of Table II. Observe that:

- 1) After adding DF-UAP or TLM-UAP, both the RCAs and the BCAs were significantly reduced, suggesting the effectiveness of DF-UAP and TLM-UAP attacks.
- 2) In most cases, TLM-UAP outperformed DF-UAP.
- 3) The BCAs of the P300 and ERN datasets were close to 0.5 after DF-UAP or TLM-UAP attacks, whereas the RCAs were lower than 0.5, implying that most test EEG trials were classified into the minority class to achieve the best attack performance.

Fig. 2 shows the number of EEG trials in each class on the three datasets, classified by EEGNet before and after applying TLM-UAP. Generally, the trials originally classified into the majority class were misclassified into the minority class after applying TLM-UAP. This is reasonable. Assume the minority class contains  $p\%$  ( $p < 50$ ) of the trials. Then, misclassifying all minority class trials into the majority class gives an ASR of  $p\%$ , whereas misclassifying all majority class trials into the minority class gives an ASR of  $(100 - p)\%$ . Clearly, the latter is larger.

An example of the EEG trial before and after applying TLM-UAP is shown in Fig. 3. TLM-UAP was so small that it is barely visible, and hence difficult to detect.

#### C. Transferability of UAP in Gray-Box Attacks

Transferability is one of the most threatening properties of adversarial examples, which means that adversarial examples generated by one model may also be able to attack another one. This section explores the transferability of DF-UAP and TLM-UAP.

A gray-box attack scenario was considered: the attacker only has access to the training set of the victim model, instead of its architecture and parameters. In this situation, the attacker can train a substitute model on the same training set to generate a UAP, which was then used to attack the victim model. The results are shown in the last part of Table II. We can observe that:

- 1) The classification performances degraded after gray-box attacks, verifying the transferability of both DF-UAP and TLM-UAP.

TABLE II  
RCAs AND BCAs OF THE THREE CNN CLASSIFIERS IN DIFFERENT NON-TARGET ATTACK SCENARIOS ON THE THREE DATASETS ( $\xi = 0.2$ ).

| Experiment     | Dataset | Victim Model | Baseline |         | White-Box Attack |                | Gray-Box Attack           |                |                |                            |                |                |
|----------------|---------|--------------|----------|---------|------------------|----------------|---------------------------|----------------|----------------|----------------------------|----------------|----------------|
|                |         |              | Clean    | Noisy   | DF-UAP           | TLM-UAP        | Substitute Model (DF-UAP) |                |                | Substitute Model (TLM-UAP) |                |                |
|                |         |              |          |         |                  |                | EEGNet                    | DeepCNN        | ShallowCNN     | EEGNet                     | DeepCNN        | ShallowCNN     |
| Within-Subject | P300    | EEGNet       | .79/.79  | .81/.79 | <b>.17/.50</b>   | <b>.17/.50</b> | .22/.52                   | .21/.52        | .59/.71        | <b>.18/.51</b>             | <b>.18/.51</b> | <b>.49/.65</b> |
|                |         | DeepCNN      | .84/.80  | .84/.81 | .18/.51          | <b>.17/.50</b> | .30/.57                   | .20/.52        | .56/.69        | <b>.21/.52</b>             | <b>.18/.51</b> | <b>.49/.64</b> |
|                |         | ShallowCNN   | .80/.77  | .80/.77 | .52/.64          | <b>.34/.56</b> | .67/.72                   | .65/.71        | .60/.68        | <b>.55/.67</b>             | <b>.48/.64</b> | <b>.44/.60</b> |
|                | ERN     | EEGNet       | .69/.63  | .69/.64 | .32/.51          | <b>.31/.50</b> | .62/.68                   | <b>.51/.59</b> | .67/.63        | <b>.57/.65</b>             | .56/.58        | <b>.64/.63</b> |
|                |         | DeepCNN      | .72/.71  | .72/.71 | <b>.41/.54</b>   | .50/.59        | .67/.69                   | <b>.53/.58</b> | .66/.67        | <b>.66/.69</b>             | .57/.59        | <b>.64/.66</b> |
|                |         | ShallowCNN   | .69/.65  | .70/.66 | .50/.52          | <b>.49/.52</b> | <b>.67/.64</b>            | <b>.60/.60</b> | <b>.57/.60</b> | .68/.65                    | .63/.61        | .60/.62        |
|                | MI      | EEGNet       | .50/.50  | .47/.48 | .30/.29          | <b>.24/.25</b> | <b>.38/.37</b>            | .37/.37        | .40/.40        | .42/.42                    | <b>.30/.30</b> | <b>.36/.36</b> |
|                |         | DeepCNN      | .55/.54  | .55/.54 | .33/.33          | <b>.26/.29</b> | <b>.54/.53</b>            | .46/.46        | .48/.47        | .54/.54                    | <b>.33/.33</b> | <b>.34/.34</b> |
|                |         | ShallowCNN   | .76/.76  | .68/.68 | .36/.36          | <b>.28/.28</b> | <b>.62/.61</b>            | .48/.48        | .38/.38        | .72/.72                    | <b>.42/.42</b> | <b>.28/.28</b> |
| Cross-Subject  | P300    | EEGNet       | .68/.63  | .69/.63 | .19/.51          | <b>.17/.50</b> | .24/.53                   | .25/.53        | .30/.55        | <b>.17/.50</b>             | <b>.17/.50</b> | <b>.20/.51</b> |
|                |         | DeepCNN      | .69/.64  | .70/.64 | .20/.51          | <b>.18/.50</b> | .32/.55                   | .22/.52        | .28/.54        | <b>.18/.50</b>             | <b>.18/.50</b> | <b>.20/.52</b> |
|                |         | ShallowCNN   | .67/.62  | .66/.62 | .27/.54          | <b>.19/.50</b> | .41/.58                   | .35/.57        | .32/.55        | <b>.28/.54</b>             | <b>.24/.52</b> | <b>.21/.51</b> |
|                | ERN     | EEGNet       | .67/.65  | .67/.65 | .31/.51          | <b>.29/.50</b> | .53/.58                   | .53/.58        | .41/.56        | <b>.32/.51</b>             | <b>.34/.51</b> | <b>.35/.53</b> |
|                |         | DeepCNN      | .65/.63  | .64/.63 | <b>.31/.50</b>   | .33/.50        | .54/.55                   | .48/.54        | .44/.56        | <b>.30/.50</b>             | <b>.34/.50</b> | <b>.34/.60</b> |
|                |         | ShallowCNN   | .68/.64  | .68/.64 | .49/.56          | <b>.29/.50</b> | .67/.61                   | .66/.59        | .53/.58        | <b>.53/.59</b>             | <b>.53/.61</b> | <b>.30/.51</b> |
|                | MI      | EEGNet       | .44/.44  | .38/.38 | .28/.28          | <b>.25/.25</b> | <b>.35/.35</b>            | .32/.32        | .33/.33        | .36/.36                    | <b>.31/.31</b> | <b>.26/.26</b> |
|                |         | DeepCNN      | .47/.47  | .44/.44 | .34/.34          | <b>.25/.25</b> | <b>.37/.37</b>            | .35/.35        | .36/.36        | .42/.42                    | <b>.31/.31</b> | <b>.29/.29</b> |
|                |         | ShallowCNN   | .47/.47  | .43/.43 | .27/.27          | <b>.25/.25</b> | <b>.30/.30</b>            | <b>.27/.27</b> | .37/.37        | .44/.44                    | .31/.31        | <b>.29/.29</b> |

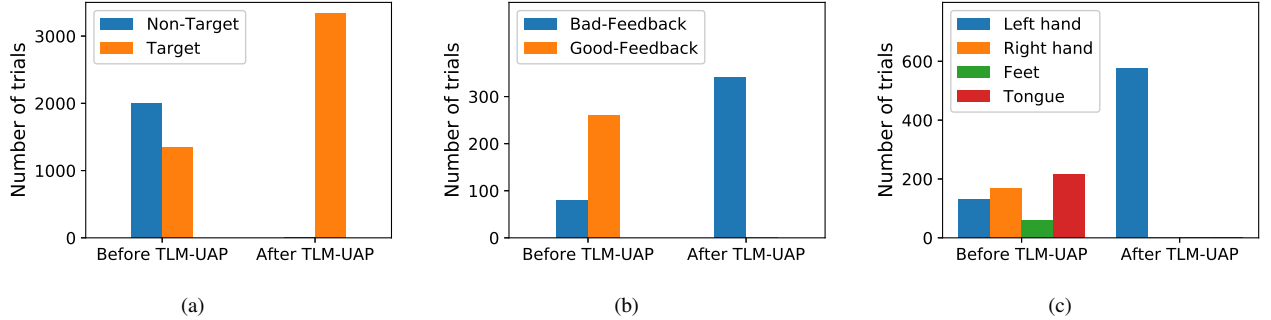


Fig. 2. Number of EEG trials in each class (classified by EEGNet), before and after applying TLM-UAP in white-box non-target attack. a) P300; b) ERN; and, c) MI.

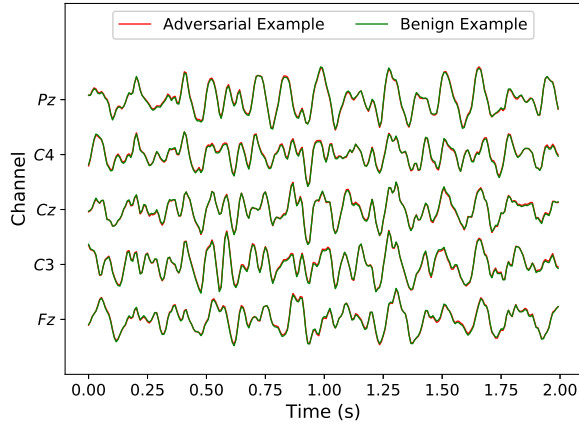


Fig. 3. An example of the EEG trial before and after the white-box non-target TLM-UAP attack on the MI dataset ( $\xi = 0.2$ ).

- 2) In most cases, TLM-UAP led to larger classification performance degradation of the RCA and BCA than DF-UAP, suggesting that our proposed TLM-UAP was more effective than DF-UAP.

#### D. Characteristics of UAP

Additional experiments were performed in this subsection to analyze the characteristics of TLM-UAP.

1) *Signal-to-Perturbation Ratio (SPR)*: We computed SPRs of the perturbed EEG trials, including applying random noise, DF-UAP and TLM-UAP in white-box attacks. We treated the original EEG trials as clean signals, and computed the SPRs in cross-subject experiments. The results are shown in Table III. In most cases, the SPRs of the adversarial examples perturbed by TLM-UAP were higher than those perturbed by DF-UAP, i.e., the UAP crafted by TLM had a smaller magnitude, and hence may be more difficult to detect. This is because in addition to  $\|v\|_p \leq \xi$ , TLM-UAP is also bounded by the constraint function  $C(x, v)$  in (7).

2) *Spectrogram*: In order to analyze the time-frequency characteristics of UAP, we compared the spectrograms of DF-UAP and TLM-UAP for the three classifiers in white-box attacks. The results are shown in Fig. 4.

DF-UAPs and TLM-UAPs share similar spectrogram patterns: for EEGNet and DeepCNN, the energy was mainly concentrated in the low-frequency areas, whereas it was more scattered for ShallowCNN. There were also some significant differences. For EEGNet, the energy of DF-UAP was con-

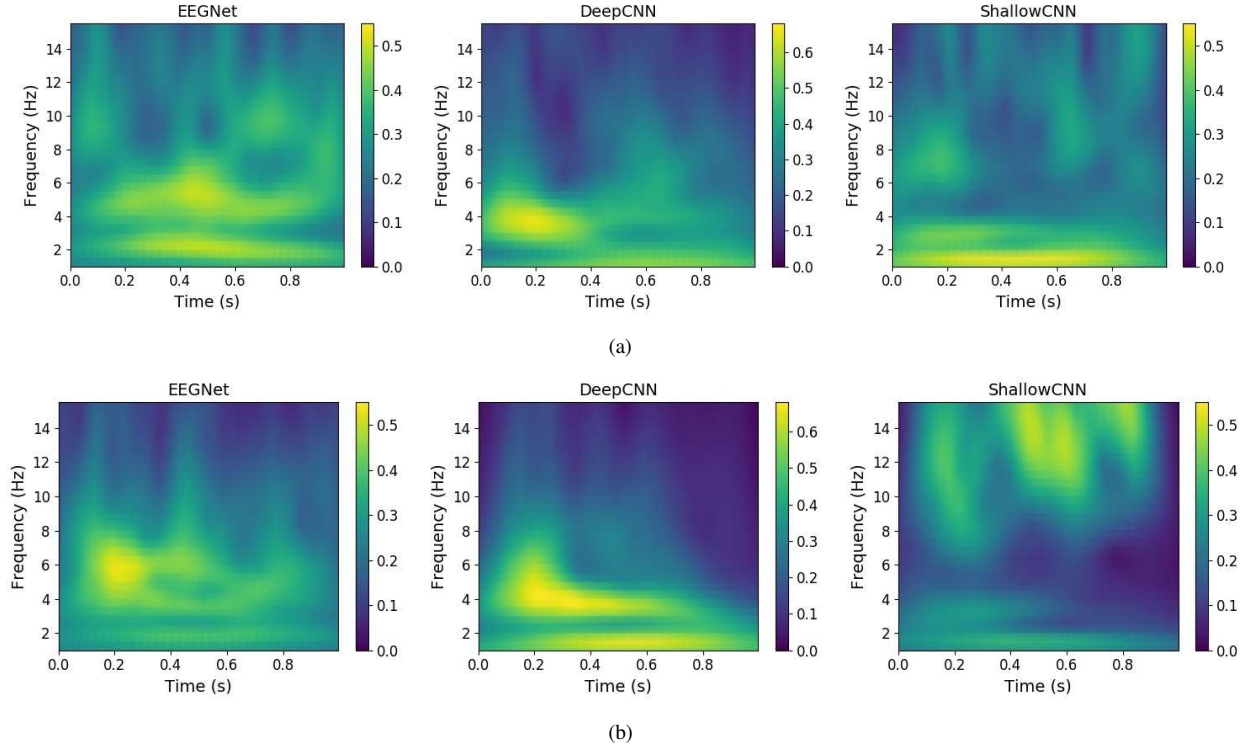


Fig. 4. Spectrograms of DF-UAPs and TLM-UAPs on the P300 dataset in white-box non-target within-subject experiments. Channel  $C_z$  was used. (a) DF-UAP; (b) TLM-UAP.

TABLE III  
SPRS (dB) OF EEG TRIALS PERTURBED BY DF-UAP AND TLM-UAP IN  
WHITE-BOX NON-TARGET ATTACKS ( $\xi = 0.2$ ).

|         | Dataset | EEGNet       | DeepCNN      | ShallowCNN   |
|---------|---------|--------------|--------------|--------------|
| DF-UAP  | P300    | 16.99        | 17.00        | 17.85        |
|         | ERN     | 16.22        | 16.73        | <b>17.73</b> |
|         | MI      | 21.71        | 13.08        | 14.57        |
| TLM-UAP | P300    | <b>21.17</b> | <b>19.92</b> | <b>20.58</b> |
|         | ERN     | <b>21.03</b> | <b>21.67</b> | 17.72        |
|         | MI      | <b>23.48</b> | <b>17.85</b> | <b>17.80</b> |

centrated in  $[0.1, 0.9]$ s and  $[0, 7]$ Hz, whereas the energy of TLM-UAP was concentrated in  $[0.1, 0.8]$ s and  $[3, 8]$ Hz. For DeepCNN, TLM-UAP seemed to affect a longer period of signals, i.e.,  $[0.4, 0.8]$ s. For ShallowCNN, TLM-UAP mainly perturbed the high-frequency areas, which were less uniform than DF-UAP.

These results also explained the cross-subject transferability results of TLM-UAP on the P300 dataset in Table II: TLM-UAPs generated from EEGNet and DeepCNN were more similar than those from ShallowCNN, so TLM-UAP generated from EEGNet (DeepCNN) was more effective in attacking DeepCNN (EEGNet), and their RCAs and BCAs were close.

### E. Hyper-Parameter Sensitivity

This subsection analyzes the sensitivity of TLM-UAP to its hyper-parameters.

1) *The Magnitude of TLM-UAP*:  $\xi$  is an important parameter in Algorithm 3, which directly bounds the magnitude of the perturbation. We evaluated the TLM-UAP attack performance

with respect to different  $\xi$ . As shown in Fig. 5, the RCA decreased rapidly as  $\xi$  increased and converged at  $\xi = 0.2$  in most cases, suggesting that a small UAP is powerful enough to attack the victim model.

2) *Training Set Size*: It's interesting to study if the training set size affects the performance of TLM-UAP. Fig. 6 shows the white-box non-target attack performance of TLM-UAP, which were trained with different numbers of EEG trials in cross-subject experiments on the MI dataset. It seems that we do not need a large training set to obtain an effective TLM-UAP. The same phenomenon was also observed in [22].

3) *Constraint*: We also compared different constraint  $C$  in (7): *No* constraint,  $L1$  regularization ( $\alpha = 10/10/5$  for EEGNet/DeepCNN/ShallowCNN), and  $L2$  regularization ( $\alpha = 100$ ). The SPRs on the three datasets are shown in Table IV. Albeit similar attack performances, TLM-UAP trained with constraints led to a larger SPR (the SPRs in the ‘L1’ and ‘L2’ rows are larger than those in the corresponding ‘No’ row).

Fig. 7 shows that adding different constraints significantly changed the waveforms of TLM-UAP.  $L1$  regularization introduced sparsity, whereas  $L2$  regularization reduced the perturbation magnitude.

We may also generate a TLM-UAP which satisfies other requirements by changing the constraint function  $C$ , such as perturbing certain EEG channels, or even against a metric function which is used to detect adversarial examples. We will leave these to our future research.

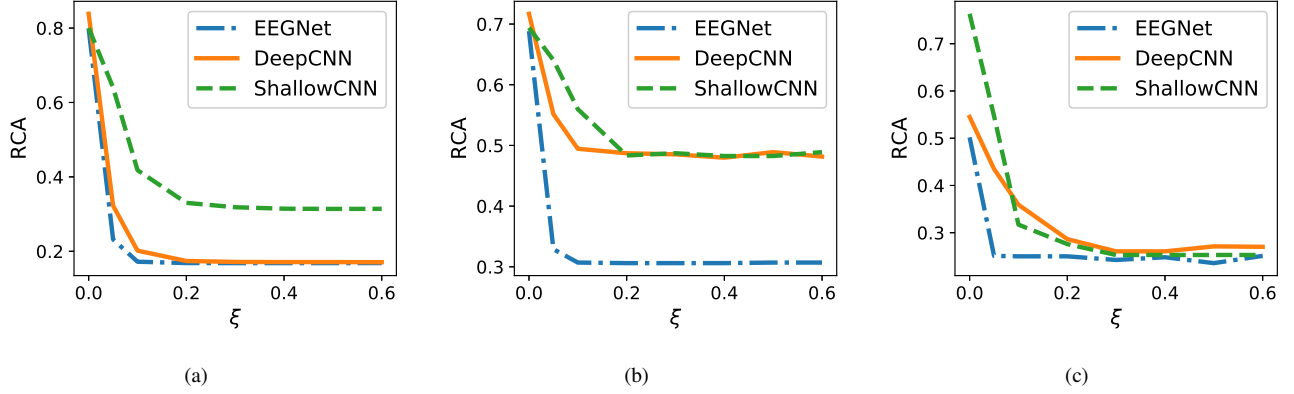


Fig. 5. RCAs of the victim model after white-box non-target within-subject TLM-UAP attack, with respect to different  $\xi$ . (a) P300 dataset; (b) ERN dataset; and, (c) MI dataset.

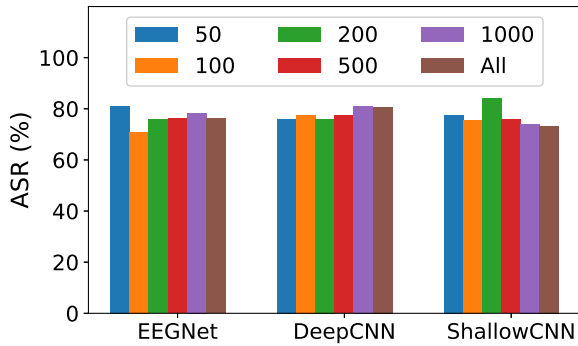


Fig. 6. ASRs in white-box non-target cross-subject experiment on the MI dataset, with respect to different training set sizes. 'All' means all 4,608 training EEG trials in the MI dataset were used in Algorithm 3.

TABLE IV  
MEAN RCAs (%) AND SPRs (dB) ON THE THREE DATASETS USING DIFFERENT CONSTRAINTS IN WHITE-BOX NON-TARGET ATTACKS ( $\xi = 0.2$ ).

| Dataset | Constraint | Mean RCA | SPR of TLM-UAP |         |            |
|---------|------------|----------|----------------|---------|------------|
|         |            |          | EEGNet         | DeepCNN | ShallowCNN |
| P300    | No         | 17.18    | 14.89          | 14.71   | 14.45      |
|         | L1         | 17.36    | 18.39          | 17.82   | 17.16      |
|         | L2         | 17.85    | 21.17          | 19.92   | 20.58      |
| ERN     | No         | 30.96    | 19.91          | 20.70   | 17.02      |
|         | L1         | 29.24    | 21.45          | 22.05   | 17.11      |
|         | L2         | 30.66    | 21.03          | 21.67   | 17.72      |
| MI      | No         | 25.05    | 22.88          | 15.46   | 16.11      |
|         | L1         | 25.08    | 23.35          | 53.76   | 16.88      |
|         | L2         | 25.06    | 23.48          | 17.85   | 17.80      |

## V. TARGET ATTACK RESULTS

Our TLM approach is also capable of performing target attacks, which can be easily achieved by changing the loss function  $l$  in (7).

We performed white-box target attacks in cross-subject experiments on the three datasets and evaluated the target rate, which is the ratio of the number of samples classified to the target class divided by the number of total samples, for each target class. The results are shown in Table V. TLM-UAPs had close to 100% target rates in white-box target attacks, indicating that our approach can manipulate the BCI systems to output whatever the attacker wants, which may be more

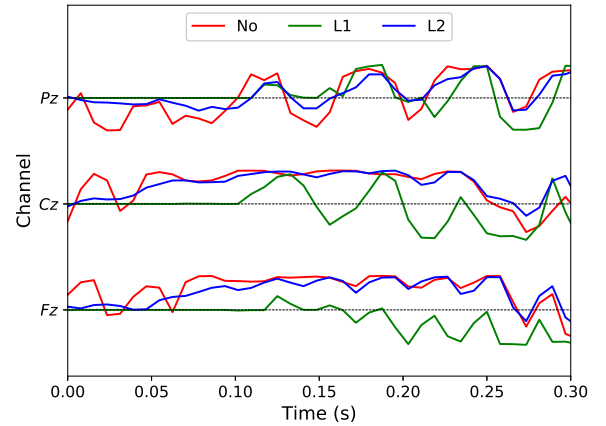


Fig. 7. TLM-UAP trained with different constraints on the MI dataset in white-box non-target attacks. Channels  $P_z$ ,  $C_z$  and  $F_z$  were used.

dangerous than non-target attacks. For example, in a BCI-driven wheelchair, a target TLM-UAP attack may force all commands to be interpreted as a specific command (e.g., going forward), and hence run the user into danger.

To our knowledge, no one has studied UAPs for target attacks before. Our TLM approach is the first in this direction.

## VI. CONCLUSIONS AND FUTURE RESEARCH

Multiple CNN classifiers have been proposed for EEG-based BCIs. However, CNN models are vulnerable to UAPs, which are small and example-independent perturbations, yet powerful enough to significantly degrade the performance of a CNN model when added to a benign example. This paper has proposed a novel TLM approach to generate UAP for EEG-based BCI systems. Experimental results demonstrated its effectiveness in attacking three popular CNN classifiers for both non-target and target attacks. We also verified the transferability of the UAPs in EEG-based BCI systems. To our knowledge, this is the first study on UAPs of CNN classifiers in EEG-based BCIs, and also first study on UAPs for target attacks. It exposes a critical security problem in BCIs, and hopefully will lead to the design of safer BCIs.

TABLE V

TARGET RATES OF THE THREE CNN CLASSIFIERS IN CROSS-SUBJECT WHITE-BOX TARGET TLM-UAP ATTACKS ON THE THREE DATASETS ( $\xi = 0.2$ ).

| Dataset | Victim Model | Target Class | Baseline |       | TLM-UAP Attack |
|---------|--------------|--------------|----------|-------|----------------|
|         |              |              | Clean    | Noisy |                |
| P300    | EEGNet       | Non-target   | .6627    | .6463 | .9629          |
|         |              | Target       | .3373    | .3510 | .9572          |
|         | DeepCNN      | Non-target   | .6755    | .6637 | .9416          |
|         |              | Target       | .3245    | .3116 | .9373          |
|         | ShallowCNN   | Non-target   | .6505    | .6597 | .8904          |
|         |              | Target       | .3495    | .3499 | .8306          |
| ERN     | EEGNet       | Bad          | .3537    | .3741 | .9980          |
|         |              | Good         | .6463    | .6300 | .9971          |
|         | DeepCNN      | Bad          | .3770    | .3309 | .9912          |
|         |              | Good         | .6230    | .6739 | .9976          |
|         | ShallowCNN   | Bad          | .3033    | .2910 | .9741          |
|         |              | Good         | .6967    | .7160 | .9888          |
| MI      | EEGNet       | Left         | .3152    | .1350 | .9821          |
|         |              | Right        | .2830    | .2056 | .9850          |
|         |              | Feet         | .1545    | .1954 | .9994          |
|         |              | Tongue       | .2473    | .5380 | 1.000          |
|         | DeepCNN      | Left         | .2535    | .1765 | .8839          |
|         |              | Right        | .3491    | .2207 | .9238          |
|         |              | Feet         | .2282    | .3155 | .9659          |
|         |              | Tongue       | .1692    | .2544 | .9938          |
|         | ShallowCNN   | Left         | .2872    | .1952 | .9151          |
|         |              | Right        | .2537    | .1746 | .9443          |
|         |              | Feet         | .2647    | .2838 | .9819          |
|         |              | Tongue       | .2124    | .3673 | .9983          |

Our future research will enhance the transferability of TLM-UAP in deep learning, and also consider how to attack traditional machine learning models in EEG-based BCIs. More importantly, we will design effective strategies to defend UAP attacks.

## REFERENCES

- [1] S. Sutton, M. Braren, J. Zubin, and E. R. John, "Evoked-potential correlates of stimulus uncertainty," *Science*, vol. 150, no. 3700, pp. 1187–1188, 1965.
- [2] L. Farwell and E. Donchin, "Talking off the top of your head: Toward a mental prosthesis utilizing event-related brain potentials," *Electroencephalography and Clinical Neurophysiology*, vol. 70, no. 6, pp. 510–523, Dec. 1988.
- [3] D. Wu, "Online and offline domain adaptation for reducing BCI calibration effort," *IEEE Trans. on Human-Machine Systems*, vol. 47, no. 4, pp. 550–563, 2017.
- [4] D. Wu, V. J. Lawhern, W. D. Hairston, and B. J. Lance, "Switching EEG headsets made easy: Reducing offline calibration effort using active weighted adaptation regularization," *IEEE Trans. on Neural Systems and Rehabilitation Engineering*, vol. 24, no. 11, pp. 1125–1137, 2016.
- [5] G. Pfurtscheller and C. Neuper, "Motor imagery and direct brain-computer communication," *Proc. IEEE*, vol. 89, no. 7, pp. 1123–1134, Jul 2001.
- [6] D. Zhu, J. Bieger, G. Garcia Molina, and R. M. Aarts, "A survey of stimulation methods used in SSVEP-based BCIs," *Computational Intelligence and Neuroscience*, p. 702357, 2010.
- [7] V. J. Lawhern, A. J. Solon, N. R. Waytowich, S. M. Gordon, C. P. Hung, and B. J. Lance, "EEGNet: A compact convolutional neural network for EEG-based brain-computer interfaces," *Journal of Neural Engineering*, vol. 15, no. 5, p. 056013, Jun. 2018.
- [8] R. T. Schirrmester, J. T. Springenberg, L. D. J. Fiederer, M. Glasstetter, K. Eggenberger, M. Tangermann, F. Hutter, W. Burgard, and T. Ball, "Deep learning with convolutional neural networks for EEG decoding and visualization," *Human Brain Mapping*, vol. 38, no. 11, pp. 5391–5420, 2017.
- [9] P. Bashivan, I. Rish, M. Yeasin, and N. Codella, "Learning representations from EEG with deep recurrent-convolutional neural networks," in *Proc. Int'l Conf. on Learning Representations*, San Juan, Puerto Rico, May 2016.
- [10] Y. R. Tabar and U. Halici, "A novel deep learning approach for classification of EEG motor imagery signals," *Journal of Neural Engineering*, vol. 14, no. 1, p. 016003, 2017.
- [11] Z. Tayeb, J. Fedjaev, N. Ghaboosi, C. Richter, L. Everding, X. Qu, Y. Wu, G. Cheng, and J. Conradt, "Validating deep neural networks for online decoding of motor imagery movements from EEG signals," *Sensors*, vol. 19, no. 1, p. 210, Jan. 2019.
- [12] C. Szegedy, W. Zaremba, I. Sutskever, J. Bruna, D. Erhan, I. J. Goodfellow, and R. Fergus, "Intriguing properties of neural networks," in *Proc. Int'l Conf. on Learning Representations*, Banff, Canada, Apr. 2014.
- [13] B. Biggio, I. Corona, D. Maiorca, B. Nelson, N. Šrđić, P. Laskov, G. Giacinto, and F. Roli, "Evasion attacks against machine learning at test time," in *Proc. Joint European Conf. on Machine Learning and Knowledge Discovery in Databases*, Berlin, Germany, Sep. 2013, pp. 387–402.
- [14] I. J. Goodfellow, J. Shlens, and C. Szegedy, "Explaining and harnessing adversarial examples," in *Proc. Int'l Conf. on Learning Representations*, San Diego, CA, May 2015.
- [15] A. Kurakin, I. J. Goodfellow, and S. Bengio, "Adversarial examples in the physical world," in *Proc. Int'l Conf. on Learning Representations*, Toulon, France, Apr. 2017.
- [16] T. B. Brown, D. Mané, A. Roy, M. Abadi, and J. Gilmer, "Adversarial patch," *CoRR*, vol. abs/1712.09665, 2017. [Online]. Available: <http://arxiv.org/abs/1712.09665>
- [17] A. Athalye, L. Engstrom, A. Ilyas, and K. Kwok, "Synthesizing robust adversarial examples," in *Proc. 35th Int'l Conf. on Machine Learning*, Stockholm, Sweden, Jul. 2018, pp. 284–293.
- [18] N. Carlini and D. A. Wagner, "Audio adversarial examples: Targeted attacks on speech-to-text," in *Proc. IEEE Symposium on Security and Privacy*, San Francisco, CA, May 2018, pp. 1–7.
- [19] K. Grosse, N. Papernot, P. Manoharan, M. Backes, and P. McDaniel, "Adversarial perturbations against deep neural networks for malware classification," *CoRR*, vol. abs/1606.04435, 2016. [Online]. Available: <https://arxiv.org/abs/1606.04435>
- [20] X. Zhang and D. Wu, "On the vulnerability of CNN classifiers in EEG-based BCIs," *IEEE Trans. on Neural Systems and Rehabilitation Engineering*, vol. 27, no. 5, pp. 814–825, May 2019.
- [21] J. Li, K. Cheng, S. Wang, F. Morstatter, R. P. Trevino, J. Tang, and H. Liu, "Feature selection: A data perspective," *CoRR*, vol. abs/1601.07996, 2016. [Online]. Available: <http://arxiv.org/abs/1601.07996>
- [22] S.-M. Moosavi-Dezfooli, A. Fawzi, O. Fawzi, and P. Frossard, "Universal adversarial perturbations," in *Proc. IEEE Conf. on Computer Vision and Pattern Recognition*, Honolulu, HI, July 2017, pp. 1765–1773.
- [23] S.-M. Moosavi-Dezfooli, A. Fawzi, and P. Frossard, "Deepfool: A simple and accurate method to fool deep neural networks," in *Proc. IEEE Conf. on Computer Vision and Pattern Recognition*, Las Vegas, NV, Jun. 2016, pp. 2574–2582.
- [24] P. Neekharu, S. Hussain, P. Pandey, S. Dubnov, J. J. McAuley, and F. Koushanfar, "Universal adversarial perturbations for speech recognition systems," *CoRR*, vol. abs/1905.03828, 2019. [Online]. Available: <http://arxiv.org/abs/1905.03828>
- [25] M. Behjati, S.-M. Moosavi-Dezfooli, M. S. Baghshah, and P. Frossard, "Universal adversarial attacks on text classifiers," in *Proc. IEEE Int'l Conf. on Acoustics, Speech and Signal Processing*, Brighton, United Kingdom, May 2019, pp. 7345–7349.
- [26] K. R. Mopuri, A. Ganeshan, and V. B. Radhakrishnan, "Generalizable data-free objective for crafting universal adversarial perturbations," *IEEE Trans. on Pattern Analysis and Machine Intelligence*, vol. 41, no. 10, pp. 2452–2465, Oct. 2019.
- [27] X. Jiang, X. Zhang, and D. Wu, "Active learning for black-box adversarial attacks in EEG-based brain-computer interfaces," in *Proc. IEEE Symposium Series on Computational Intelligence*, Xiamen, China, Dec. 2019.
- [28] U. Hoffmann, J.-M. Vesin, T. Ebrahimi, and K. Diserens, "An efficient P300-based brain-computer interface for disabled subjects," *Journal of Neuroscience Methods*, vol. 167, no. 1, pp. 115–125, Jan. 2008.
- [29] P. Margaux, M. Emmanuel, D. Sbastien, B. Olivier, and M. Jrmie, "Objective and subjective evaluation of online error correction during P300-based spelling," *Advances in Human-Computer Interaction*, vol. 2012, no. 578295, p. 13, Oct. 2012.
- [30] M. Tangermann, K.-R. Miller, A. Aertsen, N. Birbaumer, C. Braun, C. Brunner, R. Leeb, C. Mehring, K. Miller, G. Mueller-Putz, G. Nolte, G. Pfurtscheller, H. Preissl, G. Schalk, A. Schlgl, C. Vidaurre, S. Waldert, and B. Blankertz, "Review of the BCI Competition IV," *Frontiers in Neuroscience*, vol. 6, p. 55, 2012.

- [31] F. Chollet, "Xception: Deep learning with depthwise separable convolutions," in *Proc. IEEE Conf. on Computer Vision and Pattern Recognition*, Honolulu, HI, Jul. 2017, pp. 1800–1807.
- [32] K. K. Ang, Z. Y. Chin, H. Zhang, and C. Guan, "Filter bank common spatial pattern (FBCSP) in brain-computer interface," in *Proc. IEEE Int'l Joint Conf. on Neural Networks*, Hong Kong, China, Jun. 2008.
- [33] D. P. Kingma and J. Ba, "Adam: A method for stochastic optimization," *CoRR*, vol. abs/1412.6980, 2014. [Online]. Available: <https://arxiv.org/abs/1412.6980>